


Incorporation of water-derived hydrogen into methane during artificial maturation of source rock under hydrothermal conditions

 The corrections made in this section will be reviewed and approved by a journal production editor.

David T. Wang^{a,b,*}, dtw@alum.mit.edu, Jeffrey S. Seewald^b, Eoghan P. Reeves^c, Shuhei Ono^a, Sean P. Sylva^b

^aDepartment of Earth, Atmospheric and Planetary Sciences, Massachusetts Institute of Technology, Cambridge, MA 02139, USA

^bMarine Chemistry and Geochemistry Department, Woods Hole Oceanographic Institution, Woods Hole, MA 02543, USA

^cDepartment of Earth Science, University of Bergen, Bergen N-5007, Norway

*Corresponding author. Present address: Esso Exploration and Production Guyana Ltd, 86 Duke Street, Georgetown, Guyana.

Associate Editor—Clifford C Walters

Abstract

To investigate the origin of $\text{C}-\text{HC}-\text{H}$ bonds in thermogenic methane (CH_4), a solvent-extracted sample of organic-rich Eagle Ford shale was reacted with heavy water (D_2O) under hydrothermal conditions (350 bar) in a flexible Au-TiO₂ cell hydrothermal apparatus at a water-to-rock ratio of approximately 5:1. Temperature was increased from 200 to 350 °C over the course of one month and the concentrations of aqueous species and methane isotopologues were quantified as a function of time. In general, production of hydrogen, CO₂, alkanes, and alkenes increased with time and temperature. Methane formed during the early stages of the experiment at 200 °C was primarily C¹H₄ with some CH₃D. With progressively higher temperatures, increasing proportions of deuterated isotopologues were produced. Near the end of the experiment, the concentration of CD₄ exceeded that of all other isotopologues combined. These results suggest that competition between rates of kerogen-water isotopic exchange and natural gas generation may govern the D/H ratio of thermogenic gases. Furthermore, hydrogenation of kerogen by water may be responsible for hydrocarbon yields in excess of those predicted by conventional models of source rock maturation in which hydrocarbon generation is limited by the amount of organically bonded hydrogen.

Keywords:

Methane, Natural gas generation kinetics, D/H ratios, Kerogen, Clumped isotopologues, Hydrogen isotope exchange, Water isotopes

Abbreviations

No keyword abbreviations are available

1 Introduction

Variation in D/H ratios (δD) of thermogenic natural gases is often attributed to kinetically-controlled fractionation during pyrolysis of kerogen or petroleum. A number of studies have investigated how D/H ratios of methane and other hydrocarbons evolve with increasing thermal maturity (Sackett, 1978; Berner et al., 1995; Sackett and Conkright, 1997; Tang et al., 2005; Ni et al., 2011; Reeves et al., 2012). However, kinetic isotope effects involving hydrogen addition or abstraction are often large and by themselves do not explain the geologically reasonable apparent equilibrium temperatures of ~ 150 to 220 °C obtained for reservoir gases that have been studied for their clumped isotopologue compositions (Stolper et al., 2014, 2015; Wang et al., 2015; Douglas et al., 2017; Young et al., 2017; Shuai et al., 2018; Giunta et al., 2019; Labidi et al., 2020; Thiagarajan et al., 2020). There is also evidence that the δD of CH_4 approach values expected for isotopic equilibrium between CH_4 and H_2O in formation waters at temperatures characterizing reservoirs and/or mature source rocks (~ 150 to 250 °C) (Clayton, 2003; Wang et al., 2015; Xie et al., 2021), although findings of insignificant hydrogen exchange occurring under these conditions also exist (Yeh and Epstein, 1981). In order for methane samples to have approached or attained equilibrium values of $\Delta^{13}CH_3D$ and $\Delta^{12}CH_2D_2$ —parameters that describe the abundances of clumped isotopologues relative to a stochastic population of molecules containing isotopes randomly distributed amongst them—there must be a pathway by which either (i) isotopes can be exchanged amongst methane isotopologues alone, (ii) methane isotopologues exchange hydrogen with water or other organic molecules, or (iii) methane isotopologues are derived from methyl moieties which contain $C-H$ bonds that have previously exchanged with water prior to forming methane (Hoering, 1984; Smith et al., 1985; Schimmelmann et al., 1999, 2006; Lis et al., 2006).

Here, we study the origin of $C-H$ bonds in thermogenic methane by heating a powdered, solvent-extracted source rock in the presence of D_2O , and examining the degree of deuteration in the generated methane. This experiment is conceptually very similar to ones conducted by Hoering (1984), Lewan (1997), and Schimmelmann et al. (2001). The experiments in those studies were designed to track incorporation of D into bitumen and kerogen, and none specifically quantified the extent of deuteration in the produced natural gases.


2 Materials and Methods

2.1 Experimental materials and equipment

The experiments were conducted in a gold-titanium reaction cell housed within a flexible cell hydrothermal apparatus (Seyfried et al., 1987) at the Woods Hole Oceanographic Institution (WHOI). Prior to use, the titanium surfaces in contact with the reaction cell contents were heated in air for 24 h at 400 °C to form a more inert TiO_2 surface layer. The reaction cell was further pre-treated prior to loading by soaking in concentrated HCl for 4 h, followed by rinsing with water to pH neutral and drying in the oven. The exit tube of the apparatus was cleaned by forcing ~ 20 mL of MilliQ deionized water (18.2 M Ω) through, followed by ~ 20 mL concentrated HCl, ~ 100 mL water, ~ 20 mL concentrated HNO_3 , and then ~ 100 mL of water until the pH tested 7 using pH paper.

The source material for this experiment was a hand sample of Upper Cretaceous Eagle Ford Shale taken from an outcrop in Uvalde County, Texas, USA (Hentz and Ruppel, 2010). There is no known oil or gas production from the Eagle Ford in Uvalde County (Tian et al., 2013; IHS Markit Well Database, 2019). The Eagle Ford here is thermally immature ($R_o = 0.40$ – 0.55 %, Cardneaux, 2012; Cardneaux and Nunn, 2013; Harbor, 2011). The sample was powdered to < 250 μm and Soxhlet-extracted to remove bitumen and free hydrocarbons. In a subsequent step, the solvent-extracted residue was subjected to hydrochloric acid treatment to remove carbonate minerals. Elemental analysis (Table 1) of the original rock sample (UNEX), the Soxhlet-extracted rock sample (EX), and the decalcified + extracted rock sample (DECA) indicates a total organic carbon (TOC) content of ~ 2.5 % and a carbonate content of ~ 80 % by weight. The H/C atomic ratio of the decalcified rock is 2.4. This value is probably several tens of percent higher than the actual H/C ratio of isolated kerogen (not determined) given that substantial amounts of H are likely borne by clays and other minerals that were not removed (Whelan and Thompson-Rizer, 1993; Baskin, 1997).

Table 1

 The table layout displayed in this section is not how it will appear in the final version. The representation below is solely purposed for providing corrections to the table. To preview the actual presentation of the table, please view the Proof.

Elemental analysis of Eagle Ford shale powder that was either: dried but otherwise untreated (UNEX), Soxhlet-extracted (EX), or extracted + decarbonated (DECA). Values represent weight percent of the material that was ingested by the elemental analyzer. Data from C. Johnson, WHOI, 1996.


(wt%)	UNEX	EX*	DECA
C	12.1	11.0	6.23
H	0.38	0.25	1.24
N	0.18	0.17	0.74
S	0.37	<0.2	2.3

*Used in the experiment.

Geochemical data for the Eagle Ford sample can be drawn from neighboring Kinney County, Texas, where complete sections of immature Eagle Ford have been recovered by the U.S. Geological Survey (drill core GC-3; French et al., 2020) and Shell (Iona-1 drill core; Eldrett et al., 2014, 2015; Sun et al., 2016); there, the Eagle Ford also crops out, is immature, and is presumed to be geochemically similar. The high calcium carbonate content and relatively lower organic enrichment is consistent with data from the Upper Eagle Ford in the ~~Shell~~ Iona-1 core ~~from neighboring Kinney County, Texas~~ (Eldrett et al., 2015).

The reaction cell was loaded with 10.03 g of the EX powder. The starting fluid used was heavy water (D₂O, 99 % purity, Cambridge Isotope Laboratories, Inc.) containing NaCl (0.497 mol/kg). The NaCl was added to allow for detection of any leaks in the reaction cell, as dilution of the starting fluid by deionized water from the surrounding pressure vessel would decrease observed Cl concentrations. The reaction cell was loaded with 55.03 g of this starting fluid, sealed with a small argon-purged headspace (to allow for expansion of the starting fluid at conditions), and then pressurized and brought to initial condition (200 °C, 350 bar) in approximately 2 h. Several milliliters of fluid were bled during heat-up to purge the exit tube, leaving an estimated 52.6 g of fluid in the cell at the beginning of the experiment (Table 2).

Table 2

 The table layout displayed in this section is not how it will appear in the final version. The representation below is solely purposed for providing corrections to the table. To preview the actual presentation of the table, please view the Proof.

Concentration of aqueous species during heating of Soxhlet-extracted Eagle Ford shale at 200 to 350 °C and 350 bar in the presence of saline D₂O fluid.

Time Pt #	Time (h)	H ₂ (μmol/kg) ^a	CH ₄ (μmol/kg)	ΣCO ₂ (mmol/kg)	CH ₄ /ΣC ₂₋₄ ^b	ΣH ₂ S (mmol/kg)	pD (25 °C) ^c
<i>Experiment begun with 52.6 g of fluid at temperature of 200 °C</i>							
1	19	BDL (13)	1.2	4.8	0.78		
2	164	BDL (13)	3.8	10.8	1.06		
<i>Temperature raised to 300 °C</i>							
3	191	98.0	8.7	21.9	1.68		
4	284	247	235	45.8	1.30		
5	427	392	396	65.5	1.09		

<i>Injected ~18.3 g starting fluid and raised temperature to 325 °C</i>							
6	451	477	319	44.7	1.06		
7	598	791	825	45.3	0.96		
<i>Raised temperature to 350 °C</i>							
8	617	969	1.32×10^3	54.4	1.01		
9	836	1,110	3.47×10^3	51.2	1.06	18.0	5.90

Analytical uncertainties (2σ) are ± 2 °C for T ; $\pm 10\%$ for H_2 ; $\pm 5\%$ for ΣCO_2 , CH_4 , and C_2 to C_4 hydrocarbons, $\pm 2\%$ for ΣH_2S ; and ± 0.05 units for pD. Concentrations are molar quantities per kg fluid. **BDL, below detection limit ($<13 \mu\text{mol/kg}$ for H_2)**

Table Footnotes

^a Determined from thermal conductivity response calibrated against a known H_2 standard, and then multiplied by 1.35 to account for the difference in thermal conductivity between D_2 and 1H_2 (Saxena and Saxena, 1970; Whisnant et al., 2011).

^b Calculated as the molar ratio of methane to the sum of ethane, propane, isobutane, and *n*-butane.

^c The listed pD value was calculated from pH measured with a glass electrode: $pD = pH_{\text{measured}} + 0.41$ (Glasoe and Long, 1960).

2.2 Analytical methods

To monitor the fluid composition and the extent of deuteration with time, sample aliquots of fluid were withdrawn through the capillary exit tube into gastight glass/PTFE syringes. Immediately prior to a sampling event, a small amount (~0.5 g) of fluid was removed and discarded to flush the exit tube. A fluid sample was taken at the beginning and end of each temperature stage. One additional sample (#4) was drawn in the middle of the second temperature stage (300 °C). At time point #6, two aliquots were drawn, each in separate syringes and sampled into separate vials.

Deuterium (D_2) is likely to be the main form of molecular hydrogen (H_2) in our experiment due to rapid exchange between water and dissolved hydrogen (Lécluse and Robert, 1994; Wang et al., 2018). The concentration of H_2 was determined after headspace extraction using a gas chromatograph (GC) supplied with nitrogen carrier gas and equipped with a molecular sieve 5 Å column and thermal conductivity detector. Concentrations reported in Table 2 have been corrected for the difference in thermal conductivity between D_2 and 1H_2 (see note *a* of Table 2), assuming that all dissolved hydrogen is as D_2 . Analytical reproducibility of H_2 concentration data is $\pm 10\%$ or better (2σ).

Concentrations of total dissolved inorganic carbon (ΣCO_2) and C_1 to C_6 hydrocarbons (alkanes and alkenes) were determined using a purge-and-trap cryofocusing device coupled to a gas chromatograph equipped with a Porapak Q column and serially connected thermal conductivity and flame ionization detectors. Analytical procedures were as described in Reeves et al. (2012). Analytical reproducibility on duplicate samples was $\pm 5\%$ or better (2σ). The C_5 and C_6 compounds could not be quantified accurately due to their semi-volatile nature; however, C_5 and C_6 were detected at all sampling points.

At each sampling, a separate ~1 to 2 mL aliquot was injected directly into a pre-weighed, evacuated serum vial capped with boiled blue butyl rubber stoppers, for analysis of the extent of deuteration of methane. A Hewlett-Packard (HP) 6890 gas chromatography-mass spectrometry (GC-MS) system equipped with a 5 Å molecular sieve column (HP-PLOT 30 m \times 0.32 mm \times 12.0 μm) coupled to an HP 5973 mass selective detector was used to determine the amount of deuteration in CH_4 . Mass spectrometer source and quadrupole analyzer temperatures were 230 and 150 °C, respectively, and mass spectra were recorded with an electron impact (EI) ionization energy of 70 eV. Ion currents were monitored at integral masses between m/z 10 and 50. Extracted ion currents were quantified at m/z 14 through 20 for methane. Expected fragmentation patterns of the five methane- d_n isotopologues (C^1H_4 , CH_3D , CH_2D_2 , CHD_3 , and CD_4) were determined by analysis of commercial synthetic standards (>98% purity, Cambridge Isotope Laboratories, Inc.). We refer to the fully protiated methane isotopologue as C^1H_4 in the text when it is necessary to specifically distinguish it from bulk CH_4 .

3 Results and discussion

3.1 Temperature and thermal maturity

Temperatures logged during the experiment are shown in Fig. 1A. Using the temperature history, we calculated thermal maturity as a function of time in units of vitrinite reflectance ($\%R_o$) using EASY $\%R_o$ (Sweeney and Burnham, 1990). The estimated thermal maturities are plotted in Fig. 1B. While the model predicts maturities of $\sim 0.20\%$ to 0.34% R_o -equivalent for time points #1 and 2 (respectively) and the data are plotted at these calculated maturities, the actual maturity at these time points can be no **less than** $0.4\text{--}0.5\%$ (the initial maturity of the Eagle Ford rock sample). The difference between the plotted and actual $\%R_o$ values is somewhat immaterial; what is key is that time points #1 and 2 represent source rock that has undergone only incipient organic metamorphism. Maturities encountered in the remainder of the experiment spanned the entire range of the oil window (ca. 0.5% to 1.3% R_o -equivalent; Burnham, 2019). The modeled maturity at the final time point (#9) is 1.27% R_o .


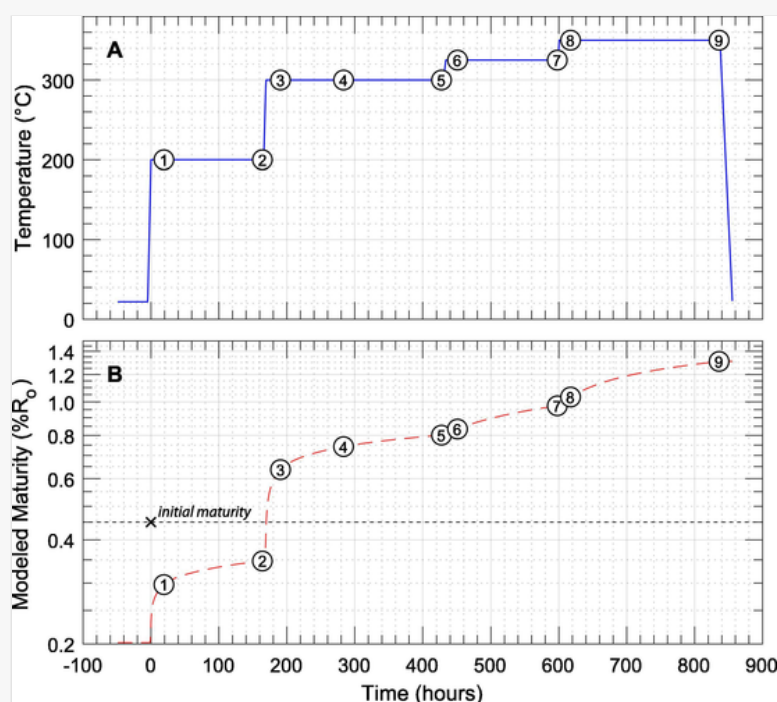
 Images are optimised for fast web viewing. Click on the image to view the original version.

Fig. 1



Profiles of (A) temperature and (B) estimated thermal maturity (calculated using EASY $\%R_o$) vs. time. Time zero ($t = 0$) is the time at which the experiment was brought to initial conditions ($200\text{ }^{\circ}\text{C}$ and 350 bar). Numbers in circles represent sampling points (Table 2).

Replacement Image: Figure 1.pdf

Replacement Instruction: Replace figure with attached. Figure width 5 inches.

3.2 Concentrations of aqueous species

3.2.1 Inorganic species

Measured concentrations of aqueous species are shown in Fig. 2. Concentrations of aqueous H_2 increased from below detection ($<13\text{ }\mu\text{mol/kg}$) to up to 1.1 mmol/kg at the end of the experiment, and increased with each temperature step. The H_2 concentration also rose slightly between the beginning and end of each temperature stage of the experiment.


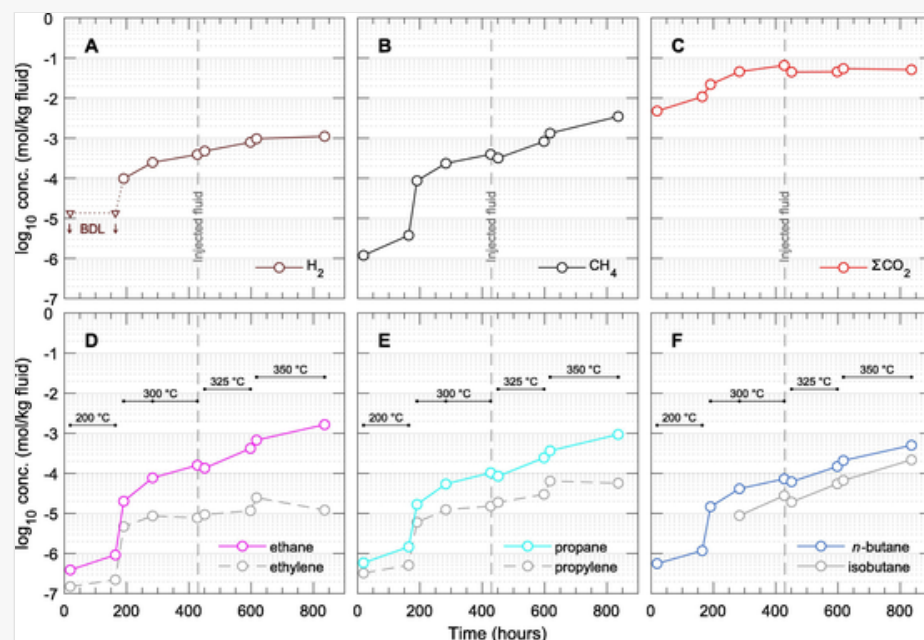
 Images are optimised for fast web viewing. Click on the image to view the original version.

Fig. 2



Concentrations of aqueous species over time during the experiment. (A) Hydrogen (H_2 , measured as D_2); (B) methane (CH_4); (C) total inorganic carbon (ΣCO_2); (D) ethane and ethylene; (E) propane and propylene; and (F) n -butane and isobutane. Note that injection of additional saline D_2O at 430 h diluted the concentration of all aqueous species by $\sim 50\%$. BDL, below detection limit ($<13 \mu\text{mol/kg}$ for D_2H_2).

Replacement Image: Figure 2.pdf

Replacement Instruction: Replace with attached. Figure width 6 inches.

The concentration of ΣCO_2 increased during the early stages of the experiment, and leveled off at $\sim 50 \text{ mmol/kg}$ at 350°C . The plateauing inorganic carbon concentration suggests that the aqueous solution reached saturation with carbonate minerals (Seewald et al., 1998), a result of CO_2 production during hydrothermal alteration of kerogen (Seewald, 2003), and dissolution of carbonate minerals initially present in the Eagle Ford shale.

3.2.2 Alkanes and alkenes

Concentrations of methane increased in every successive time step, as did concentrations of detected n -alkanes. Except for the beginning of the experiment, molar concentrations of C_1 and ΣC_{2-4} were very similar and increased almost in unison.

Alkenes (ethylene and propylene, Fig. 2D–E) rose in concentration with every increase in temperature, indicating generation of unsaturated hydrocarbons via thermolytic processes. While concentrations of n -alkanes increased monotonically from the beginning to end of each temperature stage, the concentrations of alkenes remained constant—or in the 350°C stage, trended downwards—with time during each stage. Concentrations of alkenes consistent with thermodynamic equilibrium at measured H_2 concentrations are on the order of $\sim 10^{-7.4}$ and $\sim 10^{-6.6} \text{ mol/kg}$ for ethylene and propylene, respectively, at 350°C (Shock et al., 1989; Shock and Helgeson, 1990). Measured concentrations of alkenes were ~ 2 orders of magnitude higher than alkane-alkene equilibrium predictions, indicating strong disequilibrium in the relative concentration of alkenes and alkanes. Some portion of the $\sim 10^{-6.5} \text{ mol/kg}$ of these alkenes present at time point #1 could have been indigenous to the source rock (i.e., adsorbed and leached out during initial heating).

Evidence from hydrothermal experiments suggests that metastable, reversible alkane/alkene equilibrium should be attained under hydrothermal conditions with half-equilibration times of several hundred hours or less at temperatures of 325 to 350°C (Seewald, 1994, 2001). Failure to achieve thermodynamic equilibrium within these timescales indicates that generation of thermogenic alkenes occurs concurrently with alkane/alkene hydrogen exchange. Various pyrolysis

experiments have reported alkene production (Huizinga et al., 1987; Leif and Simoneit, 2000), lending further support to the hypothesis that continued production of alkenes competes with their conversion into alkanes via hydrogenation at these temperatures and timescales and under redox conditions characterizing hydrothermal maturation of organic-rich mudrocks.

Unlike the C₂₊ alkanes, methane cannot dehydrogenate to form an alkene. Hence, hydrogen exchange of methane requires that the very stable $\text{C}-\text{H}-\text{C}$ bond be broken. Under certain conditions, generally requiring the absence of water or other catalyst poisons, methane exchanges hydrogen over certain catalytic materials such as γ -alumina at room temperature over hours to days (Sattler, 2018, and refs. therein) or with organometallic catalysts under even colder conditions (Golden et al., 2001). However, such catalysts in their active forms are not known to occur naturally in aqueous environments. Experiments conducted by Reeves et al. (2012) with aqueous methane in the presence of iron-bearing minerals in similar flexible-cell Au-TiO₂ reaction vessels revealed only minimal potential exchange over several months, even at temperatures as high as 323 °C. Recently, Turner et al. (2022) conducted a set of experiments in flexible gold-cell hydrothermal reactors with CH₄ dissolved in supercritical water at 376 to 420 °C to specifically constrain the rate of CH₄-H₂O hydrogen isotope exchange. Their results confirm that exchange occurs over timescales of hundreds of years at 300 °C and tens of years at 350 °C (half-exchange time, $\tau_{1/2}$), much longer than the duration of our experiment.

3.3 Production of deuterated methane isotopologues

Mass spectra collected for standards are shown in Fig. 3A. Relative fragment intensities were similar to those determined in early studies from the U.S. National Bureau of Standards (Dibeler and Mohler, 1950; Mohler et al., 1958). Mass spectra of samples are shown in Fig. 3B. No methane peaks of usable size could be obtained for time point #1. All other time points yielded quantifiable extracted ion chromatogram peaks.


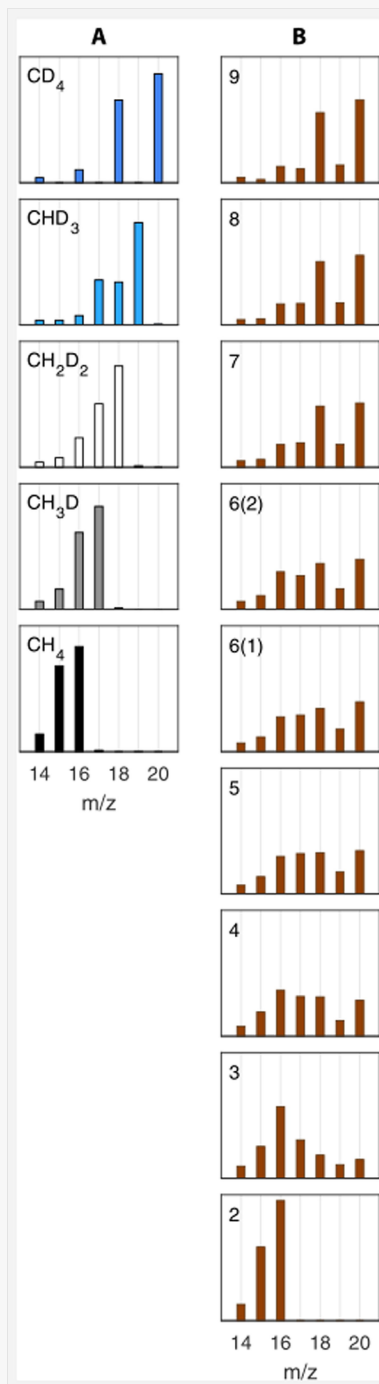
 Images are optimised for fast web viewing. Click on the image to view the original version.

Fig. 3



Mass spectra of (A) standards and (B) samples. Isotopologue is indicated in the upper left corner of each plot. Intensities were normalized such that the m/z 14 to 20 signals sum to unity. In (B), time point is indicated in the upper left corner of each plot. Two samples were taken for time point #6, hence there are two plots. No GC-MS data were obtained for time point #1.

Replacement Image: Figure 3.pdf

Replacement Instruction: This is not the correct version of the figure (looks like it was copied out of the Word document; it has the gray border). Replace figure with attached. Make the figure 8.3 inches tall. This way on the PDF, the figure caption will appear all in one column.

The mass spectra of commercial standards were used to fit the sample data using a constrained linear least-squares solver (LSQNONNEG) implemented in MATLAB.¹ Estimated fractional abundances of methane-*d* isotopologues at each

time point are shown in Fig. 4A.² While it is not straightforward to quantify the uncertainty in these fractional abundances, comparison of the calculated results for samples #6(1) and 6(2) suggests the random error is unlikely to be so large as to affect our interpretation of the overall trends below. Some systematic error is likely present as we did not correct the mass spectra for the ^{13}C isotope or for isotopic impurities in the standards. Fractional abundances for each of the isotopologues were converted into absolute abundances (Fig. 4B) by multiplying by the methane concentration. The proportion of D in methane-bound hydrogen, calculated from the relative isotopologue abundances, is shown in Fig. 5.


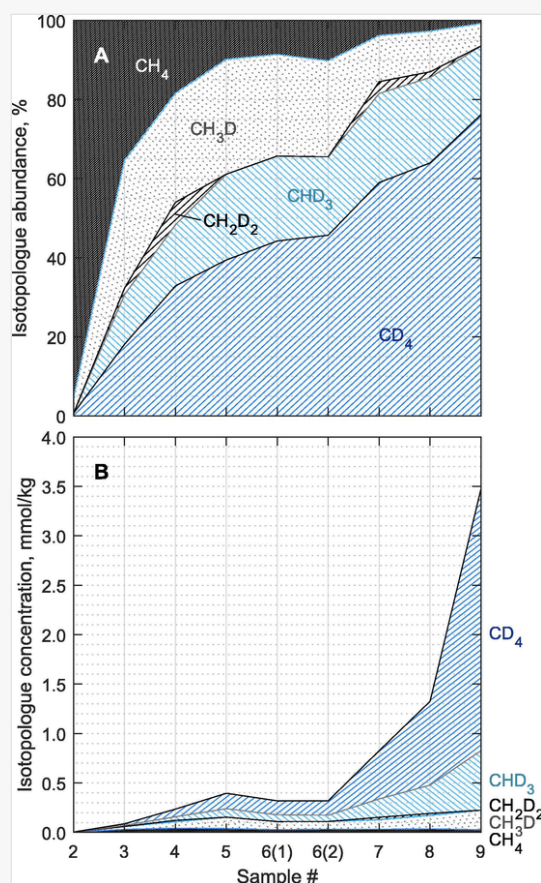
 Images are optimised for fast web viewing. Click on the image to view the original version.

Fig. 4



Calculated (A) fractional and (B) absolute abundances of methane isotopologues.

Replacement Image: Figure 4.pdf

Replacement Instruction: Replace figure with attached. This figure can be single column in PDF.


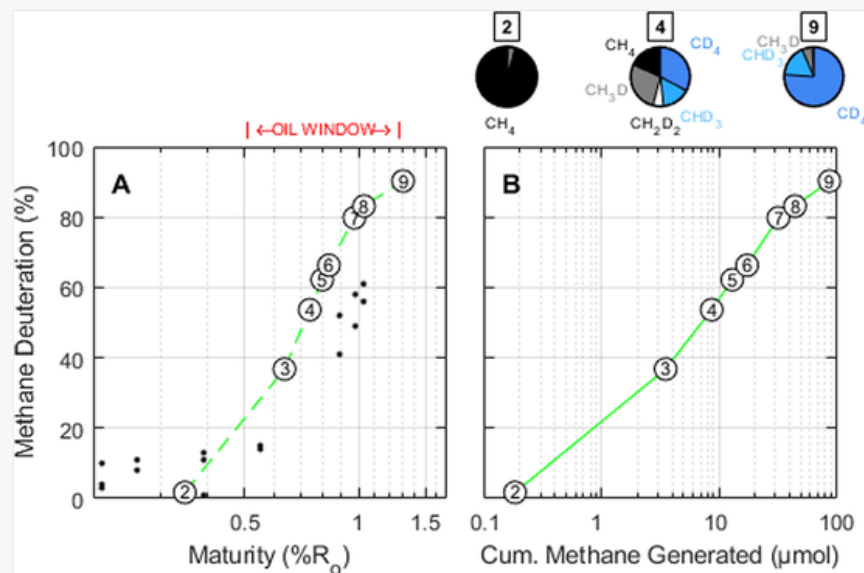
 Images are optimised for fast web viewing. Click on the image to view the original version.

Fig. 5



Extent of methane deuteration [methane-bound D/(D + H)] vs (A) estimated maturity (via EASY%Ro) and (B) cumulative methane generated. The data shown for time point #6 is the average of the two replicate samples. Small symbols in (A) are data from [Wei et al. \(2019\)](#) representing percentage of water-derived H in CH₄. Thermal maturities for the Wei et al. data were calculated from a time-temperature curve reconstructed from their described experimental procedures. Pie charts above (B) represent fractional abundances of isotopologues before, during, and after peak oil generation (time points #2, 4, and 9, respectively).

Replacement Image: Figure 5.png

Replacement Instruction: Replace figure with attached higher-res version. Figure width can be 4.5 inches.

Methane formed during the early stages of the experiment at 200 °C was primarily C¹H₄ with some CH₃D, whereas at higher temperatures the isotopologues produced consisted almost exclusively of CD₄, CHD₃, and CH₃D ([Fig. 4A](#) and [Fig. 5](#)). These results suggest that at relatively lower temperatures of ~200 °C, the rate of methane generation approaches or exceeds the rate of D/H exchange between water and kerogen, whereas at higher temperatures, extensive D/H exchange between kerogen (or petroleum, if it is also a precursor of methane) and water occurs prior to methane generation. CD₄ became the dominant methane species at temperatures of 300 °C and above, suggesting that >50% of all labile, methane-generating sites on kerogen were fully deuterated by this time. As discussed above, uncatalyzed CH₄-D₂O isotopic exchange at this temperature occurs over a much longer timescales than the short (~1 month) duration of our laboratory experiment. There is a possibility of mineral catalysis on the surfaces of the source rock powder used in the experiment, which we cannot rule out given the setup of our experiment. However, the minimal degree of isotopic exchange observed by [Reeves et al. \(2012\)](#) at temperatures of 323 °C and timescales of ~1 year in the presence of redox-active minerals (pyrite, pyrrhotite, and magnetite) suggests that direct exchange of CH₄ with D₂O in our experiment is probably unimportant.³

Production of C¹H₄ in the first stage of the experiment (200 °C) indicates that the earliest “capping” hydrogen derives from kerogen or other H-containing species in the rock as opposed to from the H atoms of water. This can only be the case if kerogen has not yet undergone D/H exchange.⁴ While constraints on timescales of D/H exchange at 200 °C are sparse, the available literature supports this assertion. Experiments conducted with model hydrocarbons indicate that D/H exchange of carbon-bound H at 200 °C takes at least several decades, much longer than the heating time in our experiment ([Sessions et al., 2004](#); [Schimmelmann et al., 2006](#); [Sessions, 2016](#); and refs. therein).

Production of C¹H₄ and CH₃D appeared to cease by midway through the 300 °C stage (time point #4, 284 h), or was overshadowed by the generation of much larger quantities of the higher isotopologues. Continued (though relatively minor) production of methane that was not fully deuterated (CHD₃ and CH₃D, [Fig. 4B](#)) suggests that the kerogen (or petroleum) from which methane was generated still did not fully exchange before methane formed.

If significant exchange were to occur, either between water and kerogen, or between water and methane generated by thermal degradation of longer chain products, and this exchange occurs sequentially, the predominant isotopologue would be expected to follow the progression C¹H₄ → CH₃D → CH₂D₂ → CHD₃ → CD₄. Instead, CH₂D₂ represents a smaller fraction of the methane isotopologues than either CH₃D or CHD₃ at all times, and calculated proportions of CH₂D₂ do not exceed 10% at any point in the experiment ([Fig. 4A](#)). A possible explanation is that

various CH_x moieties (e.g., aromatic C vs methylene C vs heteroatom-bound C) of the kerogen or generated petroleum have significantly different propensities to undergo exchange and hydrogenation (Schimmelmann et al., 2006). Thermal degradation that occurs much slower or faster than exchange may yield either fully deuterated kerogen (e.g., $-\text{CD}_3$) or singly-deuterated methane, respectively, hence leading to an absence of CH_2D_2 . Alternatively (or possibly in addition), D/H exchange of partially deuterated longer-chain hydrocarbon molecules with water may be faster than degradation, such that the production of CH_2D_2 is bypassed. The selective production of deuterated methane isotopologues is additional evidence that exchange between water/methane or methane/methane at temperatures of 200 to 350 °C is slow on timescales relevant to laboratory experiments.⁵

Comparison of our results with those of Wei et al. (2019), who examined CH_4 generation from petroleum source rock heated under hydrothermal conditions, reveals similar thermal maturity trends for the extent of CH_4 deuteration (Fig. 5A). Both studies yielded methane with an increasing percentage of water-derived hydrogen as thermal maturity increased. The deuteration vs maturity trends are sub-parallel to each other. The observed offset between the Wei et al. experimental results and ours (Fig. 5A) is probably due to the different source rocks and experimental conditions, including the use of D_2O instead of normal water as the aqueous medium in our experiments. By the middle of the oil window (0.75–0.9 % R_o), methane in both studies contained >50% of its hydrogen content derived from water.

In a differently constructed study, Dias et al. (2014) evaluated incorporation of aqueous hydrogen into gaseous products during hydrous pyrolysis of bituminous coal samples taken from a coal seam along a transect at various distances away from an igneous intrusion (and hence with different initial R_o values ranging from 0.5% to 6.8%). After hydrous pyrolysis, measured R_o values ranged from 1.4% to 6.9%. An observed dependence of δD of CH_4 to δD of water allowed them to differentiate native (sorbed or trapped) and newly-generated (via hydrous pyrolysis) hydrocarbon gases, with almost all (>90%) of CH_4 generated from coals with initial $R_o < 2.0\%$ being of newly-generated origin. While the design of their experiment did not allow for quantification of the fractional contribution of water-derived H to the hydrogen content (and hence cannot be plotted on Fig. 5A), their results are consistent with incorporation of aqueous hydrogen into hydrocarbon gases generated by maturation of thermally immature organic matter.

The percentage of methane deuteration as a function of cumulative CH_4 generated is shown in Fig. 5B.⁶ Because approximately 100 μmol of CH_4 was generated in total, the x-axis of this panel can be read as % of cumulative methane generation. At 50% deuteration, less than 10% of methane has been generated. Stated another way, for 90% of the total methane generated in the experiment, more than half of its H content comes from water. From Fig. 4A, the fully deuterated isotopologue CD_4 predominates towards the end of the experiment (time points #7–9). These late time points mark the end of the oil window (EASY%Ro between 0.9% and 1.3%) (Fig. 5A), suggesting that the immediate precursors of methane have already fully exchanged their hydrogens with water. The fourth (capping) H in methane may come directly from water or may be abstracted from deuterated kerogen (Dong et al., 2021).

3.4 Interpretation of D/H and clumped isotope signatures of thermogenic CH_4

Efforts to understand the D/H ratios of natural gas hydrocarbons have generally been focused on determining the influence of thermal maturity, organic–inorganic interactions, catalysts, and/or biological processes on the fractionation of hydrogen isotopes in these molecules during their generation, alteration, and/or destruction in source rocks and reservoirs of sedimentary basins. There exist multiple examples of quantitatively based models for predicting δD values of natural gases, each grounded in different levels of theory or empiricism (Sackett, 1978; Berner et al., 1995; Clayton, 2003; Tang et al., 2005; Lu et al., 2011, 2021; Ni et al., 2011, 2012).

Correct interpretation of δD values and clumped isotope signatures of CH_4 depends on understanding the relative kinetics of (a) methane generation from kerogen maturation or cracking of high-molecular weight hydrocarbons; (b) hydrogen exchange of methane precursor molecules with other organic molecules and/or water; and (c) direct or indirect hydrogen exchange between CH_4 and H_2O in the various rock elements of a petroleum system. Timescales of all of these processes range between years to tens of billions of years at the peak hydrocarbon-generating temperatures of 100 to 200 °C, hence the relative importance of these three processes broadly governs the amount of organic-derived and water-derived H in CH_4 . These three processes are evaluated separately here with respect to the experimental results and how they apply to the interpretation of isotope and isotopologue ratios of CH_4 .

3.4.1 Fractionation and inheritance during methane generation

Methane is generated directly during catagenesis via cleavage of methyl groups from kerogen or bitumen in source rocks. It is also produced as a product of the thermal destruction of high- and low-molecular weight free or bound hydrocarbons, low-molecular weight organic acids, and other organic molecules in source rocks and/or high-temperature reservoirs. Thermogenic methane production has been reported over a very wide range of temperatures, with some reports of commercial volumes of thermogenic natural gas generated at temperatures lower than 86 °C (Laplante, 1974), perhaps even lower than 62 °C (Rowe and Muehlenbachs, 1999). Thermal maturities of corresponding source rocks of putative low-temperature hydrocarbon gases and condensates were estimated to be as low as ~0.25% to 0.4% R_o -equivalent (Laplante, 1974; Stahl, 1977; Purcell et al., 1979; Connan and Cassou, 1980; Snowdon, 1980; Jenden et al., 1993; Muscio et al., 1994; Rowe and Muehlenbachs, 1999; Ramaswamy, 2002). Kerogen moieties will not have undergone much D/H exchange at these low thermal maturities (Dawson et al., 2005; Maslen et al., 2012; Vinnichenko et al., 2021), and thus CH_4 generated from immature or marginally-mature source rocks will partially inherit its hydrogen and their corresponding $C-H-C-H$ linkages from the precursor organic matter. Since methyl groups of wood (and presumably other naturally-occurring organic matter) carry clumped isotope values that deviate from equilibrium (Lloyd et al., 2021), and because equilibrium methyl group clumping values [$\Delta(^{13}CH_2D-R)$ values] are quite similar to $\Delta^{13}CH_3D$ values of CH_4 at these temperatures (within several tenths of a permil; Wang et al., 2015; Lloyd et al., 2021), CH_4 generated from sedimentary organic matter at low levels of thermal stress can be expected to carry non-equilibrated clumping values inherited from methane precursors (Fig. 6A). The process of terminating the $CH_3\cdot$ radical with a $H\cdot$ radical may be an additional source of disequilibrated clumped methane signatures (Dong et al., 2021; Xie et al., 2021). Under hydrothermal conditions, water is known to provide capping hydrogens to methane via a free radical mechanism (He et al., 2019). Secondary isotope effects from the breaking of $C-C-C$ bonds adjacent to intact $C-H-C-H$ bonds will also be incorporated (Ni et al., 2011).


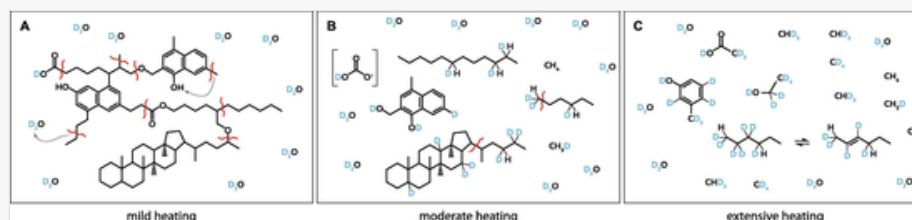
 Images are optimised for fast web viewing. Click on the image to view the original version.

Fig. 6



Cartoon showing process of sequential deuteration of sedimentary organic matter and petroleum along with generation of deuterated methane. Snapshots shown represent stages of (A) mild heating (incipient catagenesis); (B) moderate heating (oil window); and (C) extensive heating (gas window).

Replacement Image: Figure 6.pdf

Replacement Instruction: Please replace figure with attached. Figure can be single-column.

3.4.2 D/H exchange in precursor organic molecules

In maturing and thermally mature source rocks, kerogens can be expected to have exchanged part of their organic hydrogen pool with ambient waters. In experiments on source rocks heated to 310–381 °C for up to 6 days with deuterium-enriched and deuterium-depleted waters, Schimmelmann et al. (1999) found that 45% to 79% of carbon-bound hydrogen was derived from water after pyrolysis to equivalent maturities as high as ~1.3% (as EASY%Ro). Aliphatic Type I kerogen, containing large amounts of alkyl groups, were noted to be more isotopically conservative than kerogens with greater amounts of NSO-containing moieties such as Type IIS kerogen.

Exchange of n -alkyl hydrogens is slow relative to hydrogen exchange at other positions such as at the α -carbons of $C=O$ groups (Sessions et al., 2004). However, exchange rates for aliphatic hydrogens are not zero. Exchange may proceed via hydrogen transfer to a relatively stable tertiary carbocation-containing intermediate from adjacent methyl or methylene groups (Alexander et al., 1984), or via the reversible dehydration of alkanes to form alkenes under conditions of metastable equilibrium (Seewald, 1994; Reeves et al., 2012). In the absence of significant direct CH_4 -

H₂O exchange, the formation of large amounts of CD₄ during our experiment suggests that the hydrogen at methyl groups of kerogen (or in other alkyl precursors) exchanges with water under thermal conditions compatible with the generation of petroleum (Fig. 6B–C). Water is abundant within most source rocks, with even source rocks with very low water saturation containing up to several percent water by weight (Kazak and Kazak, 2019). Hence, substantial incorporation of water-derived H into CH₄ is likely to occur in actively generating source rocks so long as water is in contact with sedimentary organic matter. Water dissolved in bitumen generated from kerogen decomposition may participate in CH₄ generation (Lewan and Roy, 2011), as well as water located in pore spaces that are at least partially lined with organic matter (see Section 3.5). Equilibrium D/H fractionation between organics and water is likely to be readily attained in at least several functional groups during kerogen or bitumen maturation. While different equilibrium fractionation factors characterize the various H positions in different normal and branched alkanes, the average D/H fractionation for *n*-alkanes trends in the same direction as methane (i.e., alkane δD lower than water) (Wang et al., 2009). The progressive incorporation of pre-equilibrated alkyl H into thermogenic methane during natural gas generation may explain in part the approach towards apparent equilibrium with formation water seen in CH₄ of increasing thermal maturity (Clayton, 2003; Wang et al., 2018; Turner et al., 2021).

3.4.3 D/H exchange between methane and water in conventional vs unconventional reservoirs

Timescales of direct hydrogen exchange between CH₄ and ambient H₂O based on experiments conducted in the absence of a catalyst range from hundreds of thousands of years at temperatures around 200 °C, up to hundreds of millions of years at temperatures below 150 °C (Koepp, 1978; Reeves et al., 2012; Wang et al., 2018; Beaudry et al., 2021; Turner et al., 2022).

In a conventional petroleum system, hydrocarbons are generated within an organic-rich source rock, expelled from the source rock into permeable carrier beds, and transported along carrier beds to a reservoir or seep. Generation of oil typically occurs at 80–160 °C (the 'oil window'; Fig. 7A). Oil remains within the organic matrix until the amount of retained oil exceeds the expulsion threshold (typically considered a function of organic richness) prior to being expelled from the source rock (Sandvik et al., 1992). Oil-prone source rocks will tend to expel most of their generated hydrocarbons relatively soon after generation, whereas in leaner source rocks with less generative potential, generated oil mostly remains trapped in the source rock (Cooles et al., 1986). In the latter case, larger hydrocarbon compounds (C₁₅₊) will have ample time to both undergo exchange of its carbon-bound H (Sessions et al., 2004) and degrade to smaller compounds such as CH₄ that can more easily escape the source rock (Cooles et al., 1986). Expulsion of light hydrocarbons (C₁₅ or below, including the C₁–C₅ gases) is geologically rapid, particularly if the source rock comprises relatively thin (meter-scale) organic-rich beds interbedded with permeable silts or sands (Mackenzie et al., 1983). Secondary migration (from source rock to reservoir) is likely fast as well, even if such migration occurs over long lateral distances (~25 km) (<200,000 years for the L.A. Basin; Jung et al., 2015; see also Hindle, 1997; Eichhubl and Boles, 2000). Given that reservoirs are most often cooler than the source rocks, the C–H bonds in CH₄ will have been 'frozen' at or near the point of generation for methane generated at temperatures below ~170 °C. This is easily demonstrated using forward models of isotopic exchange such as those shown by Wang (2017, their Appendix A) for clumped isotopologues of CH₄ in conventional gases under conservative assumptions for cooling during migration. Fig. 8A shows that under a cooling rate of 50 °C/Myr—roughly 5× slower cooling than that implied by the migration timescale study of Jung et al. (2015)—and applying the CH₄–H₂O exchange kinetics determined by Turner et al. (2022), closure of methane isotopic exchange should occur around ~170 °C.⁷ Methane generated in source rocks at temperatures above the oil window (>160 °C) will be more likely to approach D/H equilibrium with water, even if it migrates immediately after generation. The dataset presented by Clayton (2003) showing a leveling-off of δD(CH₄) values at around –140 to –150 ‰ in higher thermal maturity, conventional, oil-associated gases while δ¹³C(CH₄) continues to increase is very supportive of exchange having occurred at temperatures of >170 °C within or proximal to the source rocks.


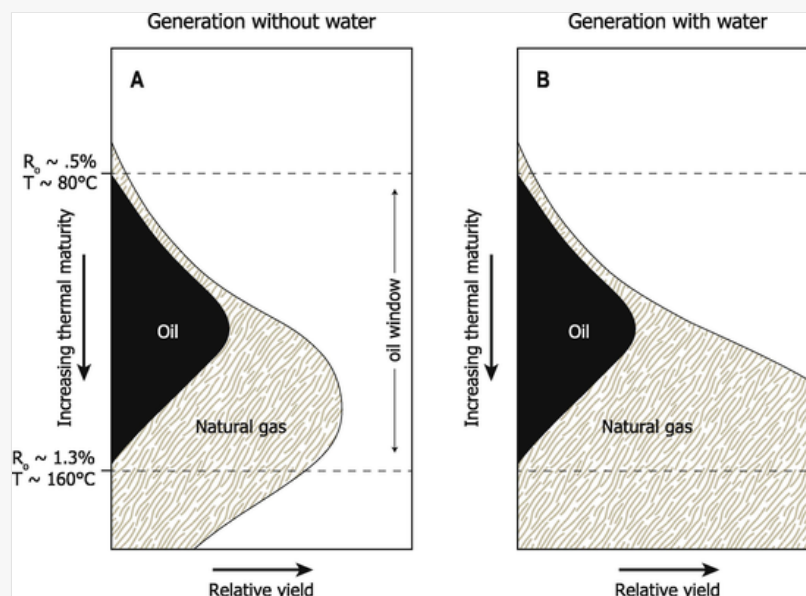
 Images are optimised for fast web viewing. Click on the image to view the original version.

Fig. 7



Schematic yields of oil and natural gas when generation occurs from source rock in the absence (A) and presence (B) of water as a source of H. (A) Traditional model of the amount and timing of organic alteration products generated during progressive burial in sedimentary basins that assumes that H in organic alteration products is derived only from kerogen and bitumen. The form of this figure is constrained by the maturation trends shown in the Van Krevelen diagram. (B) Schematic illustration of the amount and timing of organic alteration products generated if water and minerals are allowed to contribute the requisite H for the formation of hydrocarbons. Illustration is after [Seewald \(2003\)](#) and [Hunt \(1996\)](#). Listed values of % R_o and temperature are from an EASY% R_o calculation applying a heating rate of ~ 0.4 °C per Myr.

Replacement Image: Figure 7.pdf

Replacement Instruction: Replace figure with attached vector version. Figure width to remain 5.25 inches.


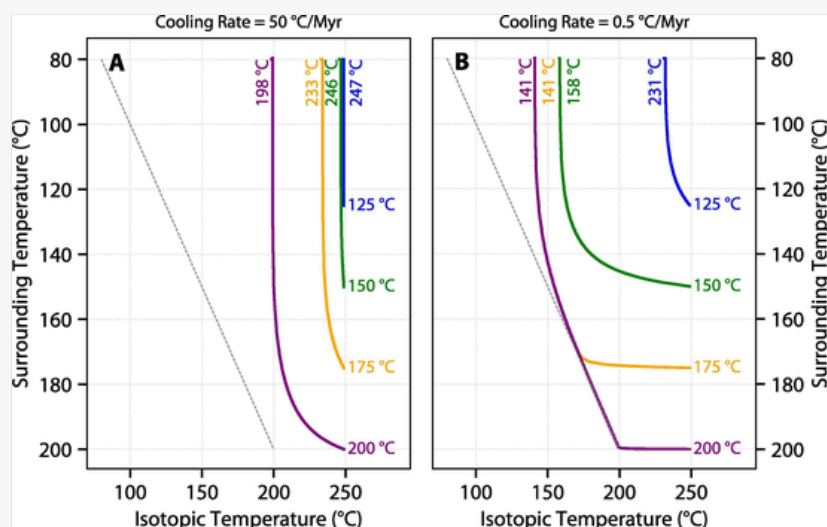
 Images are optimised for fast web viewing. Click on the image to view the original version.

Fig. 8



Influence of cooling rate on the closure temperature of hydrogen isotopic exchange between methane and water. Each fluid was cooled from an initial temperature of 125, 150, 175, or 200 °C (upright numbers at right of curves) down to a final temperature of 80 °C at a rate of either (A) 50 °C/Myr (e.g., representing migration from source to reservoir), or (B) 0.5 °C/Myr (e.g., representing gradual cooling of an unconventional, source-rock reservoir from maximum burial). The initial methane was assigned an arbitrary isotopic temperature of 250 °C in all simulations ($\Delta^{13}\text{CH}_3\text{D} \approx 2.00$ ‰). Curves show the predicted methane isotopic temperature assuming continuous exchange with 55.5 mol/L water using the kinetic parameters for $\text{CH}_4\text{-H}_2\text{O}$ exchange from [Turner et al. \(2022\)](#). Final methane isotopic temperatures are shown in rotated labels at the topmost ends of curves. The dotted gray line is a 1:1 line representing thermal equilibrium with surrounding environment.

By contrast, extensive hydrogen exchange in CH_4 likely occurs following generation for unconventional petroleum systems where the source rocks are also the reservoirs. In these self-sourced systems, CH_4 that remains entrapped in pore spaces will probably have exchanged hydrogens with surrounding organics or with any available water as long as the rock has been exposed to temperatures of at least $\sim 130^\circ\text{C}$ at maximum burial for several million years (Fig. 8B). This is supported with observations that at elevated thermal maturities, CH_4 approaches isotopic equilibrium with co-existing formation waters in unconventional reservoirs such as the Utica, Marcellus, and Eagle Ford, consistent with transfer of H from paleo-groundwaters to methane (Wang et al., 2015; Xie et al., 2021). In source-rock reservoirs which are no longer at maximum burial depths, methane may undergo retrograde isotopic exchange during cooling. Closure in these cases is highly sensitive to rates of exhumation (Reiners and Brandon, 2006), particularly as the rock passes through the range of temperatures between 130 and 160 $^\circ\text{C}$ (Fig. 8B).

3.5 Generation potential of natural gas

Volumetric calculations based on source rock extent, type, richness, and thermal maturity are used to estimate the mass of hydrocarbons generated by source rocks undergoing thermal maturation. These calculations are the basis of estimates of potential resources when assessing frontier basins when only coarse constraints on source rock presence and character are available (Schmoker, 1994). They are also formalized as programmatic subroutines embedded in modern basin modeling packages (Tissot and Espitalié, 1975; Cooles et al., 1986; Pepper and Corvi, 1995; Tissot, 2003; Freund et al., 2007; Hantschel and Kauerauf, 2009; Stainforth, 2009; Fjellanger et al., 2010) that take spatially resolved hydrogen index (HI) values of source horizons as a key input constraint.

In a series of experiments, Wenger and Price (1991) heated shale source rocks and coals in the presence of water for 30 days at temperatures of 150 to 500 $^\circ\text{C}$. They observed that HI values often increased with experimental temperature, instead of declining as would be expected for simple depletion of initial kerogen via cracking reactions. Furthermore, more hydrocarbons were generated in some experiments than the theoretical maximum yield expected if H in generated petroleum was only derived from organic matter (Price, 2001, their Fig. 3[Instruction: unlink - figure 3 here refers to a figure in the referenced paper]-Fig. 3). This excess hydrocarbon yield was attributed to incorporation of H_2O -derived hydrogen during the hydrolytic disproportionation of kerogen into $\text{CO}_2 + \text{CH}_4$ and other small paraffins, consistent with theoretical and experimental constraints on petroleum degradation in aqueous environments (Helgeson et al., 1993, 2009; Seewald, 1994, 2001, 2003).

Evidence from our results and the other studies discussed above suggest that hydrocarbon generation in source rocks may not be limited by the organic hydrogen content. Hence, if H availability is not limiting, and water participates in the formation of hydrocarbons, the upper bound on the amount of hydrocarbons that can be generated is the availability of water to petroleum-generating reactions up to the point of TOC exhaustion. This has been repeatedly suggested by several authors in years past (Lewan, 1992; Helgeson et al., 1993, 2009; Price, 1994, 2001; Seewald, 1994, 2003).⁸ If correct, kinetic models of petroleum formation employed in basin modeling that limit hydrocarbon yields based on HI values (Tissot et al., 1987; Tissot, 2003; Hantschel and Kauerauf, 2009) may significantly underpredict the true natural gas resource potential in many of the world's sedimentary basins (Fig. 7).

Chemical kinetic models employed in the upstream oil and gas industry for exploration purposes invariably use simple, pseudo-first-order reactions. Many parallel reactions may be simulated at once to simulate different classes of kerogen or petroleum breakdown products; however, all reactions are, without exception, pseudo-first-order in the mass of remaining precursor. However, as noted in Xie et al. (2022), the rate coefficients of these notionally unimolecular reactions can be pressure-dependent, because a third-body collision may be required to remove excess energy from the excited intermediates. Therefore, an algorithmic reaction mechanism generator (RMG; Allen et al., 2012)—operating from a database of elementary reaction kinetics—may be used to determine the important reactions involved in the breakdown of kerogen and petroleum, and to estimate their rate coefficients under typical subsurface pressure & temperature conditions in active source rocks. Furthermore, water is almost invariably excluded as a reactant from computational studies of the thermal decomposition of organic matter because of the computational burden involved. Examples include Class (2015) and Gao (2016) wherein geological oil-to-gas cracking was studied using RMG to simulate individual radical reactions involved in the pyrolysis of model organic compounds under dry (water-absent)

conditions. Very recent developments in RMG now allow it to handle gas- and liquid-phase heterogeneous reactions (Liu et al., 2021). In the future it may therefore be possible to extend the aforementioned studies on pyrolysis of model compounds to include H_2O as a reactant.

Several important differences between experimental hydrothermal pyrolysis of source rock powder and maturation of source rocks in nature bear discussing. Most obviously, laboratory experiments substitute higher temperatures to permit hydrocarbons to be generated within much shorter timescales than in nature. Hence, for extrapolation from laboratory to geologic conditions, it is implicitly assumed that the same chemical reactions occur in the same proportions at high and low temperatures. Experiments indicate that this is not often the case, particularly for individual compositional groups (Snowdon, 1979; Ungerer and Pelet, 1987; Dieckmann et al., 2000; Schenk and Dieckmann, 2004). Results of experimental studies, including this one, must be interpreted with this in mind.

The availability of water to natural gas-generating reactions may also differ between experiment and nature. Our experiment was set up with a comparatively high water:rock ratio (5:1) to allow ease of sampling, to maintain single-phase conditions, and to prevent dilution of the deuterium content of the water by exchange with rock. The water:carbon ratio was concomitantly high, approximately 200:1 given the TOC of 2.5% and ignoring mineral carbon, which is assumed not to participate in the generation of thermogenic methane. Grinding the Eagle Ford rock sample to rock powder allowed water to readily access exposed sedimentary organic matter. By contrast, water:rock ratios for shales existing in nature (0.003:1 to 0.23:1; Bern et al., 2021) are several orders of magnitude lower than those used in experiments. Petrophysical studies of the structure of pore systems within clay-rich, organic-rich, overmature gas shales suggest that much of the water is bound to the surfaces of clay minerals and contained predominantly in interstices between clay mineral grains (see Figure 30 in Passey et al., 2010). This clay-adsorbed “irreducible water” is considered immobile and cannot be produced during extraction of hydrocarbons, whereas free or capillary-bound water is mobile and comes comingled with gas and oil during production. Using a rastering scanning electron microscopy (SEM) technique, Passey et al. (2010) imaged overmature shale source rocks in 3D, finding abundant small ($<0.1\ \mu\text{m}$) bubble-shaped pore spaces within the organic matter and observing that this intra-organic porosity tended to be interconnected yet isolated from the water-bearing intergranular matrices.

While the physical separation of gas-containing pockets from water-bearing interstitial spaces alone might suggest that contact between water and organic material is limited, two processes must be considered. Firstly, much of the oil and gas generated at or near grain boundaries probably underwent primary migration and was expelled out of the source rock long before the present day (Mackenzie et al., 1983; Cooles et al., 1986; Sandvik et al., 1992). Hence, the absence of gas in contact with water does not necessarily indicate that water was unavailable during oil and gas generation. This is supported by more recent SEM work suggesting that a substantial amount of the water fraction in shale source rocks may have direct contact with organic matter that commonly exists within interstices of clay minerals (Gupta et al., 2018). A residual water monolayer on clay particles, if present, might be responsible for some of the undeuterated methane in the early stages of our experiment. If this is the case, using crushed rock instead of rock powder in the experiment might yield yet higher proportions of C^1H_4 in the earlier samples.

The second consideration is that trapped water may have been initially present and was quantitatively consumed during the generation of the gas now present in the organic porosity. This is analogous to water trapped within mineral interstices in partially serpentinized peridotitic rock at mid-ocean ridges reacting with the olivine minerals that surround it, resulting in often dry (waterless), H_2 - and CH_4 -rich gas secondary fluid inclusions (Klein et al., 2019; Grozeva et al., 2020). Each individual fluid inclusion (or gas-filled shale pore space), then, is a remnant micro-reactor within which all water initially present was consumed in generating the gases now present. Therefore, the activity of water in such pockets of shale source rock isolated from the broader clastic matrix may be sufficiently high to allow for hydration of kerogen at much a lower water:rock ratio in nature than used in our experiment.

4 Conclusions

Four features in the dataset are notable: (i) the production of undeuterated C^1H_4 under incipient catagenic conditions; (ii) the predominance of CD_4 towards the end of the experiment, coinciding with the late oil window; (iii) the lack of direct methane-water isotopic exchange even at $350\ ^\circ\text{C}$; and (iv) the near-absence of CH_2D_2 during the experiment. These observations suggest that while some $-\text{CH}_x$ moieties in kerogen or longer-chain hydrocarbons undergo exchange more readily than cracking, some other moieties or compound classes are much less prone to exchange.

Carefully controlled, temperature-programmed hydrous deuteration (deuterous pyrolysis or deuterothermal pyrolysis) experiments on additional source rocks and organic matter types may reveal systematic differences in the kinetics of exchangability vs hydrocarbon generation. Such experiments have the potential to improve prediction of generative yields and hydrocarbon composition in basins where timing and quality of charge are key uncertainties.

Data from this study support the hypothesis that much of the H in thermogenic natural gases may derive from water, implying that the hydrogen content of organic matter may not limit gas generation. In general, the volumetric significance of the water hydrogen reservoir hence may be underappreciated in estimations of the natural gas resource potential on Earth.


Declaration of Competing Interest

The authors declare that they have no known competing financial interests or personal relationships that could have appeared to influence the work reported in this paper.

Acknowledgments

Financial support from the U.S. National Science [Foundation](#) (NSF awards [EAR-1250394](#) to S.O.), the Alfred P. Sloan [Foundation](#) via the Deep Carbon Observatory (to S.O. and J.S.S.), a Shell-MIT Energy Initiative Fellowship, and the Kerr-McGee Professorship at MIT (to S.O.) is acknowledged. E.P.R. was supported by the Norwegian Research Council through the Centre for Geobiology (SFF Project [#179560](#)). We are grateful to Keith F. M. Thompson (PetroSurveys, Inc.) for providing the Eagle Ford rock sample, Carl Johnson (WHOI) for the elemental analyses, Aaron Sattler (ExxonMobil Research and Engineering) for advice on inverting mass spectral data, Michael Lewan (USGS) for comments on the thesis chapter from which this work originated, and Chris Clayton (CCGS) for an email exchange that inspired this study. We thank Daniel Dawson and an anonymous reviewer for helpful feedback on the manuscript, and Cliff Walters, Joe Curiale, and Lloyd Snowdon for editorial handling and additional comments. The data presented in this paper were collected while the primary author was a Ph.D. student in the [MIT/WHOI Joint](#) **Q3** Program.

References

 The corrections made in this section will be reviewed and approved by a journal production editor. The newly added/removed references and its citations will be reordered and rearranged by the production team.

Alexander, R., Kagi, R.I., Larcher, A.V., 1984. Clay catalysis of alkyl hydrogen exchange reactions—reaction mechanisms. *Organic Geochemistry* 6, 755–760.

Allen, J.W., Goldsmith, C.F., Green, W.H., 2012. Automatic estimation of pressure-dependent rate coefficients. *Physical Chemistry Chemical Physics* 14, 1131–1155.

Baskin, D.K., 1997. Atomic H/C ratio of kerogen as an estimate of thermal maturity and organic matter conversion. *AAPG Bulletin* 81, 1437–1450.

Beaudry, P., Stefánsson, A., Fiebig, J., Rhim, J.H., Ono, S., 2021. High temperature generation and equilibration of methane in terrestrial geothermal systems: Evidence from clumped isotopologues. *Geochimica et Cosmochimica Acta* 309, 209–234.

Bern, C.R., Birdwell, J.E., Jubb, A.M., 2021. Water-rock interaction and the concentrations of major, trace, and rare earth elements in hydrocarbon-associated produced waters of the United States. *Environmental Science: Processes & Impacts* 23, 1198–1219.

Berner, U., Faber, E., Scheeder, G., Panten, D., 1995. Primary cracking of algal and landplant kerogens: kinetic models of isotope variations in methane, ethane and propane. *Chemical Geology* 126, 233–245.

Burnham, A.K., 2019. Kinetic models of vitrinite, kerogen, and bitumen reflectance. *Organic Geochemistry* 131, 50–59.

Cardneaux, A.P., 2012. Mapping of the oil window in the Eagle Ford shale play of southwest Texas using thermal modeling and log overlay analysis (Masters Thesis). Louisiana State University, p. 74 pp..

Cardneaux, A., Nunn, J.A., 2013. Estimates of maturation and TOC from log data in the Eagle Ford Shale, Maverick Basin of South Texas. *Gulf Coast Association of Geological Societies Transactions* 63, 111–124.

Class, C.A., 2015. Predicting organosulfur chemistry in fuel sources (PhD Thesis). Massachusetts Institute of Technology 152 pp.

Clayton, C., 2003. Hydrogen isotope systematics of thermally generated natural gas. *International Meeting on Organic Geochemistry*, 21st. Kraków, Poland, Book of Abstracts Part I, 51–52.

Connan, J., Cassou, A.M., 1980. Properties of gases and petroleum liquids derived from terrestrial kerogen at various maturation levels. *Geochimica et Cosmochimica Acta* 44, 1–23.

Cooles, G., Mackenzie, A., Quigley, T., 1986. Calculation of petroleum masses generated and expelled from source rocks. *Organic Geochemistry* 10, 235–245.

Dawson, D., Grice, K., Alexander, R., 2005. Effect of maturation on the indigenous δD signatures of individual hydrocarbons in sediments and crude oils from the Perth Basin (Western Australia). *Organic Geochemistry* 36, 95–104.

Dias, R.F., Lewan, M.D., Birdwell, J.E., Kotarba, M.J., 2014. Differentiation of pre-existing trapped methane from thermogenic methane in an igneous-intruded coal by hydrous pyrolysis. *Organic Geochemistry* 67, 1–7.

Dibeler, V.H., Mohler, F.L., 1950. Mass spectra of the deuteromethanes. *Journal of Research of the National Institute of Standards and Technology* 45, 441–444.

Dieckmann, V., Horsfield, B., Schenk, H.J., 2000. Heating rate dependency of petroleum-forming reactions: implications for compositional kinetic predictions. *Organic Geochemistry* 31, 1333–1348.

Dong, G., Xie, H., Formolo, M., Lawson, M., Sessions, A., Eiler, J., 2021. Clumped isotope effects of thermogenic methane formation: insights from pyrolysis of hydrocarbons. *Geochimica et Cosmochimica Acta* 303, 159–183.

Douglas, P.M., Stolper, D.A., Eiler, J.M., Sessions, A.L., Lawson, M., Shuai, Y., Bishop, A., Podlaha, O.G., Ferreira, A.A., Neto, E.V.S., [Niemann, M.](#), [Steen, A.S.](#), [Huang, L.](#), [Chimiak, L.](#), [Valentine, D.L.](#), [Fiebig, J.](#), [Luhmann, A.J.](#), [Seyfried, W.E., Jr.](#), [Etiope, G.](#), [Schoell, M.](#), ~~et al.~~ [Inskeep, W.P.](#), [Moran, J.J.](#), [Kitchen, N.](#), 2017. Methane clumped isotopes: Progress and potential for a new isotopic tracer. *Organic Geochemistry* 113, 262–282.

Eichhubl, P., Boles, J.R., 2000. Rates of fluid flow in fault systems; evidence for episodic rapid fluid flow in the Miocene Monterey Formation, coastal California. *American Journal of Science* 300, 571.

Eldrett, J.S., Minisini, D., Bergman, S.C., 2014. Decoupling of the carbon cycle during Ocean Anoxic Event 2. *Geology* 42, 567–570.

Eldrett, J.S., Ma, C., Bergman, S.C., Lutz, B., Gregory, F.J., Dodsworth, P., Phipps, M., Hardas, P., Minisini, D., Ozkan, A., Ramezani, J., Bowring, S.A., Kamo, S.L., Ferguson, K., Macaulay, C., Kelly, A.E., 2015. An astronomically calibrated stratigraphy of the Cenomanian, Turonian and earliest Coniacian from the Cretaceous Western Interior Seaway, USA: Implications for global chronostratigraphy. *Cretaceous Research* 56, 316–344.

Fjellanger, E., Kontorovich, A.E., Barboza, S.A., Burshtein, L.M., Hardy, M.J., Livshits, V.R., 2010. Charging the giant gas fields of the NW Siberia basin. In: Vining, B.A., Pickering, S.C. (Eds.), *Petroleum Geology: From Mature Basins to New Frontiers – Proceedings of the 7th Petroleum Geology Conference*. Geological Society of London. pp. 659–668.

French, K.L., Birdwell, J.E., Lewan, M.D., 2020. Trends in thermal maturity indicators for the organic sulfur-rich Eagle Ford Shale. *Marine and Petroleum Geology* 118, 104459.

Freund, H., Walters, C.C., Kelemen, S.R., Siskin, M., Gorbaty, M.L., Curry, D.J., Bence, A.E., 2007. Predicting oil and gas compositional yields via chemical structure–chemical yield modeling (CS-CYM): Part 1 – Concepts and implementation. *Organic Geochemistry* 38, 288–305.

Gao, C.W., 2016. Automatic reaction mechanism generation (PhD Thesis). Massachusetts Institute of Technology, 204 pp.

Giunta, T., Young, E.D., Warr, O., Kohl, I., Ash, J.L., Martini, A., Mundle, S.O., Rumble, D., Pérez-Rodríguez, I., Wasley, M., LaRowe, D.E., Gilbert, A., Sherwood Lollar, B., 2019. Methane sources and sinks in continental sedimentary systems: New insights from paired clumped isotopologues $^{13}\text{CH}_3\text{D}$ and $^{12}\text{CH}_2\text{D}_2$. *Geochimica et Cosmochimica Acta* 245, 327–351.

Glasoe, P.K., Long, F.A., 1960. Use of glass electrodes to measure acidities in deuterium oxide. *The Journal of Physical Chemistry* 64, 188–190.

Golden, J.T., Andersen, R.A., Bergman, R.G., 2001. Exceptionally low-temperature carbon–hydrogen/carbon–deuterium exchange reactions of organic and organometallic compounds catalyzed by the $\text{Cp}^*(\text{PMe}_3)\text{IrH}(\text{ClCH}_2\text{Cl})^+$ cation. *Journal of the American Chemical Society* 123, 5837–5838.

Grozeva, N.G., Klein, F., Seewald, J.S., Sylva, S.P., 2020. Chemical and isotopic analyses of hydrocarbon-bearing fluid inclusions in olivine-rich rocks. *Philosophical Transactions of the Royal Society A: Mathematical, Physical and Engineering Sciences* 378, 20180431.

Gupta, I., Jernigen, J., Curtis, M., Rai, C., Sondergeld, C., 2018. Water-wet or oil-wet: Is it really that simple in shales? *Petrophysics - The SPWLA Journal of Formation Evaluation and Reservoir Description* 59, 308–317.

Hantschel, T., Kauerauf, A.I., 2009. Petroleum Generation. In: *Fundamentals of Basin and Petroleum Systems Modeling*. Springer, Berlin Heidelberg, Berlin, Heidelberg, pp. 151–198.

Harbor, R.L., 2011. Facies characterization and stratigraphic architecture of organic-rich mudrocks, Upper Cretaceous Eagle Ford Formation, South Texas. University of Texas at Austin, p. 195 pp. Masters Thesis.

He, K., Zhang, S., Mi, J., Fang, Y., Zhang, W., 2019. Carbon and hydrogen isotope fractionation for methane from non-isothermal pyrolysis of oil in anhydrous and hydrothermal conditions. *Energy Exploration & Exploitation* 37, 1558–1576.

Helgeson, H.C., Knox, A.M., Owens, C.E., Shock, E.L., 1993. Petroleum, oil field waters, and authigenic mineral assemblages Are they in metastable equilibrium in hydrocarbon reservoirs. *Geochimica et Cosmochimica Acta* 57, 3295–3339.

Helgeson, H.C., Richard, L., McKenzie, W.F., Norton, D.L., Schmitt, A., 2009. A chemical and thermodynamic model of oil generation in hydrocarbon source rocks. *Geochimica et Cosmochimica Acta* 73, 594–695.

Hentz, T.F., Ruppel, S.C., 2010. Regional lithostratigraphy of the Eagle Ford Shale: Maverick Basin to East Texas Basin. *Gulf Coast Association of Geological Societies Transactions* 60, 325–337.

Hindle, A.D., 1997. Petroleum Migration Pathways and Charge Concentration: A Three-Dimensional Model. *AAPG Bulletin* 81, 1451–1481.

Hoering, T., 1984. Thermal reactions of kerogen with added water, heavy water and pure organic substances. *Organic Geochemistry* 5, 267–278.

Huizinga, B.J., Tannenbaum, E., Kaplan, I.R., 1987. The role of minerals in the thermal alteration of organic matter—IV. Generation of *n*-alkanes, acyclic isoprenoids, and alkenes in laboratory experiments. *Geochimica et Cosmochimica Acta* 51, 1083–1097.

Hunt, J.M., 1996. *Petroleum Geochemistry and Geology*, 2nd ed. WH Freeman San Francisco, p. 617.

Jenden, P.D., Drazan, D.J., Kaplan, I.R., 1993. Mixing of thermogenic natural gases in northern Appalachian Basin. *AAPG Bulletin* 77, 980–998.

Jung, B., Garven, G., Boles, J.R., 2015. The geodynamics of faults and petroleum migration in the Los Angeles basin, California. *American Journal of Science* 315, 412–459.

Kazak, E.S., Kazak, A.V., 2019. A novel laboratory method for reliable water content determination of shale reservoir rocks. *Journal of Petroleum Science and Engineering* 183, 106301.

Klein, F., Grozeva, N.G., Seewald, J.S., 2019. Abiotic methane synthesis and serpentinization in olivine-hosted fluid inclusions. *Proceedings of the National Academy of Sciences* 116, 17666.

Koepp, M., 1978. D/H isotope exchange reaction between petroleum and water: a contributory determinant for D/H-isotope ratios in crude oils. The Fourth International Conference, Geochronology, Cosmochronology, Isotope Geology USGS Open-File Report 78–701, 221–222.

Labidi, J., Young, E.D., Giunta, T., Kohl, I.E., Seewald, J., Tang, H., Lilley, M.D., Früh-Green, G.L., 2020. Methane thermometry in deep-sea hydrothermal systems: Evidence for re-ordering of doubly-substituted isotopologues during fluid cooling. *Geochimica et Cosmochimica Acta* 288, 248–261.

Laplante, R.E., 1974. Hydrocarbon generation in Gulf Coast Tertiary sediments. *AAPG Bulletin* 58, 1281–1289.

Lécluse, C., Robert, F., 1994. Hydrogen isotope exchange reaction rates: Origin of water in the inner solar system. *Geochimica et Cosmochimica Acta* 58, 2927–2939.

Leif, R.N., Simoneit, B.R., 2000. The role of alkenes produced during hydrous pyrolysis of a shale. *Organic Geochemistry* 31, 1189–1208.

Lewan, M., 1992. Water as a source of hydrogen and oxygen in petroleum formation by hydrous pyrolysis. American Chemical Society, Division of Fuel Chemistry Preprint Papers 37, 1643–1649.

Lewan, M., 1997. Experiments on the role of water in petroleum formation. *Geochimica et Cosmochimica Acta* 61, 3691–3723.

Lewan, M.D., Roy, S., 2011. Role of water in hydrocarbon generation from Type-I kerogen in Mahogany oil shale of the Green River Formation. *Organic Geochemistry* 42, 31–41.

Lis, G.P., Schimmelmann, A., Mastalerz, M., 2006. D/H ratios and hydrogen exchangeability of type-II kerogens with increasing thermal maturity. *Organic Geochemistry* 37, 342–353.

Liu, M., Grinberg Dana, A., Johnson, M.S., Goldman, M.J., Jocher, A., Payne, A.M., Grambow, C.A., Han, K., Yee, N.W., Mazeau, E.J., Blondal, K., West, R.H., Goldsmith, C.F., Green, W.H., 2021. Reaction Mechanism Generator v3.0: Advances in Automatic Mechanism Generation. *Journal of Chemical Information and Modeling* 61, 2686–2696.

Lloyd, M.K., Eldridge, D.L., Stolper, D.A., 2021. Clumped $^{13}\text{CH}_3\text{D}$ and $^{12}\text{CH}_2\text{D}_2$ compositions of methyl groups from wood and synthetic monomers: Methods, experimental and theoretical calibrations, and initial results. *Geochimica et Cosmochimica Acta* 297, 233–275.

Lu, S.-F., Feng, G.-Q., Shao, M.-L., Li, J.-J., Xue, H.-T., Wang, M., Chen, F.-W., Li, W.-B., Pang, X.-T., 2021. Kinetics and fractionation of hydrogen isotopes during gas formation from representative functional groups. *Petroleum Science* 18, 1021–1032.

Lu, S., Wang, M., Xue, H., Li, J., Chen, F., Xu, Q., 2011. The impact of aqueous medium on gas yields and kinetic behaviors of hydrogen isotope fractionation during organic matter thermal degradation. *Acta Geologica Sinica - English Edition* 85, 1466–1477.

Mackenzie, A.S., Leythaeuser, D., Schaefer, R.G., Bjorøy, M., 1983. Expulsion of petroleum hydrocarbons from shale source rocks. *Nature* 301, 506–509.

IHS Markit Well Database, 2019. IHS Markit.

Maslen, E., Grice, K., Dawson, D., Wang, S., Horsfield, B., 2012. Stable hydrogen isotopes of isoprenoids and n-alkanes as a proxy for estimating the thermal history of sediments through geological time. In: Harris, N.B., Peters, K.E. (Eds.), *Analyzing the Thermal History of Sedimentary Basins: Methods and Case Studies*. SEPM Society for Sedimentary Geology, pp. 29–43.

Mohler, F.L., Dibeler, V.H., Quinn, E., 1958. Redetermination of mass spectra of deuteromethanes. *Journal of Research of the National Bureau of Standards* 61, 171–172.

Muscio, G.P.A., Horsfield, B., Welte, D.H., 1994. Occurrence of thermogenic gas in the immature zone—implications from the Bakken in-source reservoir system. *Organic Geochemistry* 22, 461–476.

Ni, Y., Ma, Q., Ellis, G.S., Dai, J., Katz, B., Zhang, S., Tang, Y., 2011. Fundamental studies on kinetic isotope effect (KIE) of hydrogen isotope fractionation in natural gas systems. *Geochimica et Cosmochimica Acta* 75, 2696–2707.

Ni, Y., Liao, F., Dai, J., Zou, C., Zhu, G., Zhang, B., Liu, Q., 2012. Using carbon and hydrogen isotopes to quantify gas maturity, formation temperature, and formation age — specific applications for gas fields from the Tarim basin, China. *Energy Exploration & Exploitation* 30, 273–293.

Passey, Q.R., Bohacs, K., Esch, W.L., Klimentidis, R., Sinha, S., 2010. From Oil-Prone Source Rock to Gas-Producing Shale Reservoir - Geologic and Petrophysical Characterization of Unconventional Shale Gas

Reservoirs, In: SPE-131350-MS. Society of Petroleum Engineers, Beijing, China, p. 29.

Pepper, A.S., Corvi, P.J., 1995. Simple kinetic models of petroleum formation. Part I: oil and gas generation from kerogen. *Marine and Petroleum Geology* 12, 291–319.

Price, L.C., 1994. Metamorphic free-for-all. *Nature* 370, 253–254.

Price, L.C., 2001. A possible deep-basin-high-rank gas machine via water-organic-matter redox reactions, i. In: Dyman, T.S., Kuuskraa, V.A. (Eds.), *Geologic Studies of Deep Natural Gas Resources*, Digital Data Series. U. S, Geological Survey.

Purcell, L.P., Rashid, M.A., Hardy, I.A., 1979. Geochemical characteristics of sedimentary rocks in Scotian basin. *AAPG Bulletin* 63, 87–105.

Ramaswamy, G., 2002. A field evidence for mineral-catalyzed formation of gas during coal maturation. *Oil & Gas Journal* 100, 32–36.

Reeves, E.P., Seewald, J.S., Sylva, S.P., 2012. Hydrogen isotope exchange between *n*-alkanes and water under hydrothermal conditions. *Geochimica et Cosmochimica Acta* 77, 582–599.

Rowe, D., Muehlenbachs, K., 1999. Low-temperature thermal generation of hydrocarbon gases in shallow shales. *Nature* 398, 61–63.

Sackett, W.M., 1978. Carbon and hydrogen isotope effects during the thermocatalytic production of hydrocarbons in laboratory simulation experiments. *Geochimica et Cosmochimica Acta* 42, 571–580.

Sackett, W.M., Conkright, M., 1997. Summary and re-evaluation of the high-temperature isotope geochemistry of methane. *Geochimica et Cosmochimica Acta* 61, 1941–1952.

Sandvik, E.I., Young, W.A., Curry, D.J., 1992. Expulsion from hydrocarbon sources: the role of organic absorption. *Organic Geochemistry* 19, 77–87.

Sattler, A., 2018. Hydrogen/Deuterium (H/D) exchange catalysis in alkanes. *ACS Catalysis* 8, 2296–2312.

Saxena, S.C., Saxena, V.K., 1970. Thermal conductivity data for hydrogen and deuterium in the range 100–1100 degrees C. *Journal of Physics A: General Physics* 3, 309–320.

Schenk, H.J., Dieckmann, V., 2004. Prediction of petroleum formation: the influence of laboratory heating rates on kinetic parameters and geological extrapolations. *Marine and Petroleum Geology* 21, 79–95.

Schimmelmann, A., Lewan, M.D., Wintsch, R.P., 1999. D/H isotope ratios of kerogen, bitumen, oil, and water in hydrous pyrolysis of source rocks containing kerogen types I, II, IIS, and III. *Geochimica et Cosmochimica Acta* 63, 3751–3766.

Schimmelmann, A., Boudou, J.-P., Lewan, M.D., Wintsch, R.P., 2001. Experimental controls on D/H and $^{13}\text{C}/^{12}\text{C}$ ratios of kerogen, bitumen and oil during hydrous pyrolysis. *Organic Geochemistry* 32, 1009–1018.

Schimmelmann, A., Sessions, A.L., Mastalerz, M., 2006. Hydrogen isotopic (D/H) composition of organic matter during diagenesis and thermal maturation. *Annual Review of Earth and Planetary Sciences* 34, 501–

Schmoker, J.W., 1994. Volumetric calculation of hydrocarbons generated. In: Magoon, L.B., Dow, W.G. (Eds.), *The Petroleum System—from Source to Trap*. AAPG Memoir, pp. 323–326.

Seewald, J.S., 1994. Evidence for metastable equilibrium between hydrocarbons under hydrothermal conditions. *Nature* 370, 285–287.

Seewald, J.S., 2001. Aqueous geochemistry of low molecular weight hydrocarbons at elevated temperatures and pressures: constraints from mineral buffered laboratory experiments. *Geochimica et Cosmochimica Acta* 65, 1641–1664.

Seewald, J.S., 2003. Organic–inorganic interactions in petroleum-producing sedimentary basins. *Nature* 426, 327–333.

Seewald, J.S., Benitez-Nelson, B.C., Whelan, J.K., 1998. Laboratory and theoretical constraints on the generation and composition of natural gas. *Geochimica et Cosmochimica Acta* 62, 1599–1617.

Sessions, A.L., 2016. Factors controlling the deuterium contents of sedimentary hydrocarbons. *Organic Geochemistry* 96, 43–64.

Sessions, A.L., Sylva, S.P., Summons, R.E., Hayes, J.M., 2004. Isotopic exchange of carbon-bound hydrogen over geologic timescales. *Geochimica et Cosmochimica Acta* 68, 1545–1559.

Seyfried, W.E., Jr., Janecky, D.R., Berndt, M.E., 1987. Rocking autoclaves for hydrothermal experiments, II. The flexible reaction-cell system. *Hydrothermal Experimental Techniques* 9, 216–239.

Shock, E.L., Helgeson, H.C., 1990. Calculation of the thermodynamic and transport properties of aqueous species at high pressures and temperatures: Standard partial molal properties of organic species. *Geochimica et Cosmochimica Acta* 54, 915–945.

Shock, E.L., Helgeson, H.C., Sverjensky, D.A., 1989. Calculation of the thermodynamic and transport properties of aqueous species at high pressures and temperatures: Standard partial molal properties of inorganic neutral species. *Geochimica et Cosmochimica Acta* 53, 2157–2183.

Shuai, Y., Etiope, G., Zhang, S., Douglas, P.M., Huang, L., Eiler, J.M., 2018. Methane clumped isotopes in the Songliao Basin (China): New insights into abiotic vs. biotic hydrocarbon formation. *Earth and Planetary Science Letters* 482, 213–221.

Smith, J., Rigby, D., Gould, K., Hart, G., Hargraves, A., 1985. An isotopic study of hydrocarbon generation processes. *Organic Geochemistry* 8, 341–347.

Snowdon, L.R., 1979. Errors in extrapolation of experimental kinetic parameters to organic geochemical systems: Geologic notes. *AAPG Bulletin* 63, 1128–1134.

Snowdon, L., 1980. Resinite—A potential petroleum source in the upper Cretaceous/Tertiary of the Beaufort-Mackenzie Basin. In: Miall, A.D. (Ed.), *Facts and Principles of World Petroleum Occurrence*. CSPG Special Publications, pp. 509–521.

Stahl, W.J., 1977. Carbon and nitrogen isotopes in hydrocarbon research and exploration. *Chemical Geology* 20, 121–149.

Stainforth, J.G., 2009. Practical kinetic modeling of petroleum generation and expulsion. *Marine and Petroleum Geology* 26, 552–572.

Stolper, D.A., Lawson, M., Davis, C.L., Ferreira, A.A., Santos Neto, E.V., Ellis, G.S., Lewan, M.D., Martini, A.M., Tang, Y., Schoell, M., Sessions, A.L., Eiler, J.M., 2014. Formation temperatures of thermogenic and biogenic methane. *Science* 344, 1500–1503.

Stolper, D., Martini, A., Clog, M., Douglas, P., Shusta, S., Valentine, D., Sessions, A., Eiler, J., 2015. Distinguishing and understanding thermogenic and biogenic sources of methane using multiply substituted isotopologues. *Geochimica et Cosmochimica Acta* 161, 219–247.

Sun, X., Zhang, T., Sun, Y., Milliken, K.L., Sun, D., 2016. Geochemical evidence of organic matter source input and depositional environments in the lower and upper Eagle Ford Formation, south Texas. *Organic Geochemistry* 98, 66–81.

Sweeney, J.J., Burnham, A.K., 1990. Evaluation of a simple model of vitrinite reflectance based on chemical kinetics. *AAPG Bulletin* 74, 1559–1570.

Tang, Y., Huang, Y., Ellis, G.S., Wang, Y., Kralert, P.G., Gillaizeau, B., Ma, Q., Hwang, R., 2005. A kinetic model for thermally induced hydrogen and carbon isotope fractionation of individual *n*-alkanes in crude oil. *Geochimica et Cosmochimica Acta* 69, 4505–4520.

Thiagarajan, N., Xie, H., Ponton, C., Kitchen, N., Peterson, B., Lawson, M., Formolo, M., Xiao, Y., Eiler, J., 2020. Isotopic evidence for quasi-equilibrium chemistry in thermally mature natural gases. *Proceedings of the National Academy of Sciences* 117, 3989–3995.

Tian, Y., Ayers, W.B., McCain, D., Jr., 2013. The Eagle Ford Shale play, south Texas: regional variations in fluid types, hydrocarbon production and reservoir properties. *IPTC 2013: International Petroleum Technology Conference. European Association of Geoscientists & Engineers p. IPTC 16808.*

Tissot, B., 2003. Preliminary data on the mechanisms and kinetics of the formation of petroleum in sediments. computer simulation of a reaction flowsheet. *Oil & Gas Science and Technology - Revue d'IFP Energies Nouvelles* 58, 183–202.

Tissot, B., Espitalié, J., 1975. L'évolution thermique de la matière organique des sédiments: applications d'une simulation mathématique. Potentiel pétrolier des bassins sédimentaires de reconstitution de l'histoire thermique des sédiments. *Revue de l'Institut Français du Pétrole* 30, 743–778.

Tissot, B., Pelet, R., Ungerer, P., 1987. Thermal history of sedimentary basins, maturation indices, and kinetics of oil and gas generation. *AAPG Bulletin* 71, 1445–1466.

Turner, A.C., Korol, R., Eldridge, D.L., Bill, M., Conrad, M.E., Miller, T.F., Stolper, D.A., 2021. Experimental and theoretical determinations of hydrogen isotopic equilibrium in the system CH₄-H₂-H₂O from 3 to 200 °C. *Geochimica et Cosmochimica Acta* 314, 223–269.

Turner, A.C., Pester, N.J., Bill, M., Conrad, M.E., Knauss, K.G., Stolper, D.A., 2022. Experimental determination of hydrogen isotope exchange rates between methane and water under hydrothermal conditions. *Geochimica et Cosmochimica Acta* 329, 231–255.

Ungerer, P., Pelet, R., 1987. Extrapolation of the kinetics of oil and gas formation from laboratory experiments to sedimentary basins. *Nature* 327, 52–54.

Vinnichenko, G., Jarrett, A.J.M., van Maldegem, L.M., Brocks, J.J., 2021. Substantial maturity influence on carbon and hydrogen isotopic composition of *n*-alkanes in sedimentary rocks. *Organic Geochemistry* 152, 104171.

Wang, Y., Sessions, A.L., Nielsen, R.J., Goddard, W.A., III, 2009. Equilibrium 2H/1H fractionations in organic molecules. II: Linear alkanes, alkenes, ketones, carboxylic acids, esters, alcohols and ethers. *Geochimica et Cosmochimica Acta* 73, 7076–7086.

Wang, D.T., Gruen, D.S., Lollar, B.S., Hinrichs, K.-U., Stewart, L.C., Holden, J.F., Hristov, A.N., Pohlman, J.W., Morrill, P.L., Könneke, M., Delwiche, K.B., Reeves, E.P., Sutcliffe, C.N., Ritter, D.J., Seewald, J.S., McIntosh, J.C., Hemond, H.F., Kubo, M.D., Cardace, D., Hoehler, T.M., Ono, S., 2015. Nonequilibrium clumped isotope signals in microbial methane. *Science* 348, 428–431.

Wang, D.T., Reeves, E.P., McDermott, J.M., Seewald, J.S., Ono, S., 2018. Clumped isotopologue constraints on the origin of methane at seafloor hot springs. *Geochimica et Cosmochimica Acta* 223, 141–158.

Wang, D.T., 2017. The geochemistry of methane isotopologues (PhD Thesis). Massachusetts Institute of Technology and Woods Hole Oceanographic Institution, 144 pp. doi:10.1575/1912/9052.

Wei, L., Gao, Z., Mastalerz, M., Schimmelmann, A., Gao, L., Wang, X., Liu, X., Wang, Y., Qiu, Z., 2019. Influence of water hydrogen on the hydrogen stable isotope ratio of methane at low versus high temperatures of methanogenesis. *Organic Geochemistry* 128, 137–147.

Wenger, L., Price, L., 1991. Differential petroleum generation and maturation paths of the different organic matter types as determined by hydrous pyrolysis over a wide range of experimental temperatures. In: In: European Association of Organic Geochemists 15th International Meeting, Advances and Applications in the Natural Environment: Organic Geochemistry. pp. 335–339.

Whelan, J.K., Thompson-Rizer, C.L., 1993. Chemical methods for assessing kerogen and protokerogen types and maturity. In: Engel, M.H., Macko, S.A. (Eds.), *Organic Geochemistry: Principles and Applications*. Springer, US, Boston, MA, pp. 289–353.

Whisnant, C.S., Hansen, P.A., Kelley, T.D., 2011. Measuring the relative concentration of H₂ and D₂ in HD gas with gas chromatography. *Review of Scientific Instruments* 82, 024101.

Xie, H., Dong, G., Formolo, M., Lawson, M., Liu, J., Cong, F., Mangenot, X., Shuai, Y., Ponton, C., Eiler, J., 2021. The evolution of intra- and inter-molecular isotope equilibria in natural gases with thermal maturation. *Geochimica et Cosmochimica Acta* 307, 22–41.

Xie, H., Formolo, M., Eiler, J., 2022. Predicting isotopologue abundances in the products of organic catagenesis with a kinetic Monte-Carlo model. *Geochimica et Cosmochimica Acta* 327, 200–228.

Yang, Y., Zhong, N., Wu, J., Pan, Y., 2022. Deep-basin gas generation via organic–inorganic interactions: New insights from redox-controlled hydrothermal experiments at elevated temperature. *International Journal of Coal Geology* 257, 104009. doi:10.1016/j.coal.2022.104009.

Yeh, H.-W., Epstein, S., 1981. Hydrogen and carbon isotopes of petroleum and related organic matter. *Geochimica et Cosmochimica Acta* 45, 753–762.

Young, E.D., Kohl, I.E., Lollar, B.S., Etiope, G., Rumble, D., Li, S., Haghnegahdar, M.A., Schauble, E.A., McCain, K.A., Foustoukos, D.I., Sutcliffe, C., Warr, O., Ballentine, C.J., Onstott, T.C., Hosgormez, H., Neubeck, A., Marques, J.M., Pérez-Rodríguez, I., Rowe, A.R., LaRowe, D.E., Magnabosco, C., Yeung, L.Y., Ash, J.L., Bryndzia, L.T., 2017. The relative abundances of resolved ¹²CH₂D₂ and ¹³CH₃D and mechanisms controlling isotopic bond ordering in abiotic and biotic methane gases. *Geochimica et Cosmochimica Acta* 203, 235–264.

Footnotes

Text Footnotes

- [1] This deconvolution scheme has been used to derive concentrations of methane-*d* isotopologues from mass spectral data for a separate experimental exchange study (A. Sattler, pers. comm.).
- [2] Results of this experiment were first presented in the appendix of a Ph.D. thesis (Wang, 2017). That earlier analysis contained a mathematical error (neglected to divide by the relative peak areas of the pure isotopologue standards). As a result, Fig. B.3 of that thesis appears different than Fig. 4 in this paper.
- [3] While it is not an important factor in exchange between CH₄ and D₂O, the source rock matrix is likely important as a catalyst for the exchange of kerogen-bound H with D₂O (prior to methane generation), a process discussed in §3.4.2 and in Alexander et al. (1984).
- [4] It is conceivable that the C¹H₄ observed at time point #2 may have been gas originally present but sorbed to a solid phase at the start of the experiment and later leached into the fluid, but we consider this unlikely because Soxhlet extraction should have removed nearly all of the CH₄ initially sorbed. Furthermore, the concentration of methane tripled between time points #1 (19-h) and #2 (164h). ~~Release of sorbed gases was probably nearly complete by 19h. h) and #2 (164 h).~~ Release of sorbed gases was probably nearly complete by 19 h.
- [5] This might be verified by heating normal water (¹H₂O) in the presence of an initial charge of CD₄ and monitoring for any increase in the δD value of water.
- [6] Calculated as $[\text{CH}_4] \times V_{\text{remaining}} + \sum([\text{CH}_4] \times V_{\text{withdrawn}})$.
- [7] More comprehensive discussions of closure (quenching) temperatures for D/H exchange reactions of CH₄ can be found in Wang et al. (2018), Turner et al. (2022), and references therein.
- [8] *Note added in proof:* A recent paper by [Instruction: Please make Yang et al. (2022) an active reference in footnote 8.]Yang et al. (2022) reports artificial maturation experiments conducted with mineral redox buffers in spatial isolation from kerogen. Their results suggest that generation of natural gas depends in part on the redox state (*f*_{H2}) of aqueous fluids in contact with kerogen, which implies a substantial role for water-derived H in the generation of light hydrocarbons.

Highlights

- Source rocks ~~were~~ creas reacted with D₂O under hydrothermal conditions.
 - Generated methane incorporated substantial amounts of deuterium.
 - Much of the hydrogen in thermogenic natural gases may derive from water.
 - Gas generation may not be limited by the HI of sedimentary organic matter.
-

Queries and Answers

Q1

Query: Please review the **given names and surnames** to make sure that we have identified them correctly and that they are presented in the desired order. Carefully verify the spelling of all authors' names as well. If changes are needed, please provide the edits in the author section. /

Answer: Reviewed

Q2

Query: Your article is being processed as a regular item to be included in a regular issue. Please confirm if this is correct or if your article should be published in a special issue using the responses below. /

Answer: Yes

Q3

Query: Correctly acknowledging the primary **funders and grant IDs** of your research is important to ensure compliance with funder policies. Please make sure that funders are mentioned accordingly. Sandvik, Sweden; Foundation, United States? /

Answer: Reviewed